International Journal of Nanoelectronics and Materials
IJNeaM
ISSN 1985-5761 | E-ISSN 2232-1535

Smart self-assembled polymeric-MMT/*Moringa Oleifera L.* particles by solvent replacement method

Rahimah Othman[a, b] *, Koh Qi Sheng[a], Mohd Irfan Hatim Mohd Dzahir[a], Monisha Devi[a], Siti Pauliena Mohd Bohari[c,d]

[a] *Faculty of Chemical Engineering & Technology, Universiti Malaysia Perlis (UniMAP), Arau 02600, Perlis, Malaysia*
[b] *Centre of Excellence for Biomass Utilization (CoEBU), Universiti Malaysia Perlis (UniMAP), 02600 Arau, Perlis, Malaysia*
[c] *Department of Bioscience, Faculty of Science, Universiti Teknologi Malaysia, 81310 Johor Bahru, MALAYSIA*
[d] *Cosmetic and Fragrance Laboratory, Institute of Bioproduct Development, Universiti Teknologi Malaysia, 81310 Johor Bahru, Malaysia*
** Corresponding author. Tel.: +60-122683052; fax: +604-97988751; e-mail: rahimah@unimap.edu.my*

Received 18 January 2024, Revised 16 March 2024, Accepted 7 May 2024

ABSTRACT

Obesity, stemming from metabolic syndrome and energy imbalance, is a common health concern characterized by excess energy consumption and fat buildup. Moringa Oleifera L. (MO), known for its anti-obesity properties, is extracted via Soxhlet extraction. MO is extracted using the Soxhlet extraction method. To evaluate the antioxidant properties of MO powder, several analyses were conducted, including the assessment of total phenolic content (TPC), total flavonoid content (TFC), 2,2'-azino-bis (3-ethylbenzothiazoline-6-sulphonic acid) (ABTS) activity, and 2,2-diphenyl-1-picrylhydrazyl (DPPH) activity. The TPC and TFC, DPPH activity, and ABTS activity values were determined to be 386.7 mg GAE/g and 82.33 mg QE/g, 32.86 %, and 49.4 % respectively. To improve drug delivery, the freeze-dried MO powder was encapsulated within a polymeric carrier, poly(ε-caprolactone) (PCL). Moreover, the incorporation of montmorillonite (MMT) into the MO-loaded PCL nanoparticles enhanced the encapsulation efficiency and drug loading of MO. Nanoprecipitation was employed as a method to produce the nanoparticles, and the effects of four key parameters were studied: the ratio of aqueous phase volume to organic volume (1.5 – 10), stirring speed (400 rpm – 1200 rpm), mass weightage of MO (1 % -5 %), and mass weightage of MMT (2 % - 5 %). Design Expert was utilized for full factorial analysis to assess the impact of these parameters on encapsulation efficiency and drug loading. The optimal formulation was achieved at the ratio of aqueous phase volume to the organic volume of 1.5, stirring speed of 400 rpm, mass weightage of MO at 1 %, and mass weightage of MMT at 5% The expected encapsulation efficiency is 91.33 % and drug loading is 6.49 %.

Keywords: *Nanoparticles, Moringa Oleifera L., Nanoprecipitation, Encapsulation, Self-assembling*

1. INTRODUCTION

Moringa Oleifera L. (MO) has been found to have many pharmacological properties such as anti-obesity, antioxidant, anti-allergic, antiasthmatic, anti-ulcer, antiepileptic, and antipyretic effects [1]. High content of flavonoids, glucosinolate, and glucoside are the main reasons for high biological activity [2]. One of the most important pharmacological activities of MO is anti-obesity. *In-vivo*, *in-vitro*, clinical studies had been carried out to study the ability of MO extracts to anti-obesity. The compounds found to be useful are astragalin, quercetin, isoquercetin, and quercetin-3-O-malonylglucoside [3]

A big wheel in producing powdered herbal extracts is to control the particle size, the surface properties, and the release of pharmacological drugs to achieve the site-specific action of the active ingredients at the therapeutically optimal rate and dose regimen. The size of herbal particulates is designed to effectively spread the active ingredients (herbals) throughout the human body quickly without blood occlusion and untimely drug leakage [4]. In fact, many drugs are insoluble in aqueous media and biological fluids and, thus, their effects are diminished due to poor bioavailability.

To enhance their solubility, drug molecules can be incorporated in the interlayer space of layered clays, known as montmorillonite (MMT), which is a natural clay mineral with a thickness of individual layers of ≤1 nm [5]. MMT exhibits high drug loading capacity due to high specific surface area and provides mucoadhesive properties required for drug delivery across the gastrointestinal barrier. Thus, nanoparticlization provides unique advantages based on different synthetic strategies, with targeting moiety that can achieve targeted drug delivery to minimize side effects. The poor water-solubility of anti-obesity drugs can be addressed via nano-encapsulation [6].

There are numerous methods used for the fabrication of polymeric nanoparticles such as salting out, spray drying, desolvation, dialysis, and nanoprecipitation [7]. Nanoprecipitation, also known as the solvent displacement method, is a method to prepare NPs that is a simple, easy, fast, and reproducible one-step method. A solvent and a non-solvent polymer are necessary for the process of nanoprecipitation. Typically, a volatile organic solvent and water are used for this purpose. Both liquids must be miscible with one another. When the polymer solution is

mixed with an excessive amount of the non-solvent, nearly instantaneous formation of the NPs occurs. The solvent is then removed by evaporation [8]. The energy required by this process is not high and can be scaled up easily. Nanoprecipitation can be done in a relatively short time, inexpensive, and no precursor emulsion is needed [9]. Non-halogenated organic solvent can be used in nanoprecipitation which gives smaller PNPs than emulsion-solvent evaporation. The use of non-halogenated organic solvents is less toxic than halogenated solvents [10].

To improve the transportation of therapeutic molecules, sophisticated drug delivery systems based on "smart" composite nanoparticles (NPs) have been developed recently. The advancement of nanoparticles with thoughtful design has the potential to improve medication targeting, solubility, prolonged circulation, and tissue penetration [11]. Thus, in this study, the incorporation of adhesive cationic MMTs onto the biodegradable poly(ε-caprolactone) matrix was discovered to potentially serve as 'smart' features. These features facilitate the entrapment of more MO into the confined space of PCL (poly(ε-caprolactone)) nanoparticles, thereby prolonging the release duration of MO in specific pH environments.

The prime focus of this ongoing project is to examine the synthesis of smart-assembled organoclay PCL nanoparticles for hypercholesterolemia and obesity treatments. MO leaf extract has pharmacological properties for anti-obesity and anti-hypercholesterolemia drugs due to the presence of some phytochemical compounds such as isoquercetin and astragalin. The encapsulated *Moringa Oleifera L.* (MO) extract onto NPs matrix would also improve the active surface area, stability, bioavailability, reduce oxidation, control the release of antioxidant compounds, as well as mask the appearance and bitter taste of herbal extracts. Thus, a highly MO-loaded adsorptive smart-assembled MMT dispersion into poly(*ε*-caprolactone) nanoparticles matrix will be introduced in this study (hereafter known as MO-loaded MMT/PCL NPs).

2. MATERIALS AND METHODS

2.1. Chemicals

Acetone (Ace, purity ≥ 99.98 %) and poly(ε-caprolactone) (PCL, M_w = 14,000 g mol^{-1} with a glass transition temperature of 60 °C) were purchased from Sigma-Aldrich. Other chemicals, like methanol, acetone, ethanol, ethyl acetate, sodium chloride, quercetin, gallic acid, Folin-Ciocalteu reagent, aluminum chloride, sodium nitrate, sodium nitrate, sodium carbonate, 2,2-diphenyl-1-picrylhydrazyl (DPPH), 2,2'-azino-bis- [3-ethylbenzothiazoline sulphonate] (ABTS) (all for purity of 90 % to 95 % purity) were purchased from R&M Chemicals, Malaysia. Distilled water acts as the aqueous phase in Soxhlet extraction. The MO leaves will be collected from the wild shrub regions in Perlis. All leaves are selected based on similar size (ca. 15 – 20 mm × 10 mm) and color. The organic phase was a homogeneous solution containing 1 g L^{-1} (1000 ppm) of the polymer at the specific portions of MO and MMT in Ace.

2.2. Methods

2.2.1 MO Powder Preparation

The MO leaves were collected with their stems still attached. These detached leaves were then washed thoroughly with ap water to remove any dirt or impurities. Following the washing step, the leaves were soaked in a 0.9 % sodium chloride solution for 15 minutes. Subsequently, the leaves were rinsed once again with tap water to eliminate any remaining traces of the sodium chloride solution. To ensure proper drying, the rinsed leaves were left to dry naturally for four days at room temperature. These dried leaves were then subjected to blending, using a suitable blender or grinder. The resulting powder was carefully sieved to obtain a fine powder with a particle size of approximately 250 µm. The powdered MO was finally stored in an airtight dark container to protect it from exposure to light, moisture, and air, which could potentially degrade its quality over time. The moisture content of the leaves after drying is calculated with Equation 1, with where M_{before} and M_{after} are mass of leaves before and after drying, respectively.

$$Initial\ moisture\ content\ (\%) = \frac{M_{before} - M_{after}}{M_{before}} \times 100\% \qquad (1)$$

2.2.2 MO Extraction Procedures

The extraction of MO powder was conducted in Soxhlet extraction. 5 g of MO powder was accurately weighed out. The powder was then placed inside an extractor thimble. 167 mL of distilled water was measured and poured into a beaker. A mixture of aqueous methanol (42 mL) and acetone (126 mL) was prepared in a ratio of 1:3, and the solution was added to the beaker containing the distilled water. The mixture was refluxed using the heating mantle at 80 °C - 90 °C for 240 minutes, with the input of the heating mantle set around 150 and not exceeding 300. The timing started when the solvent began to boil. The extracted yield was then concentrated using a rotary evaporator for 15 minutes and stored in a refrigerator at 5 °C to maintain its stability and potency. The concentrated MO extract was powdered by Lanconco FreeZone 4.5 Liter -50C Benchtop Freeze Dryer -46 °C for 2 days at the Institute of Sustainable Agrotechnology (INSAT), UniMAP. The freeze-dried MO powder was obtained and stored in a desiccator immediately for further use.

2.2.3 Total Phenolic Content Analysis

The working solution at different concentrations (1, 2.5, 5, 10, 15 ppm) was measured at 765 nm using a UV-visible spectrophotometer. A calibration curve was obtained with a linear equation of $y = 0.0018x + 0.0696$, $R^2 = 0.9981$. To prepare the sample, 0.1 mL of extract and 0.2 mL of Folin-Ciocalteu reagent were added to 8 mL of distilled water. The mixture was incubated at room temperature for 3 minutes, after which 1 mL of 20 % sodium carbonate was added. The resulting solution was then left in the dark for 30 minutes. Subsequently, the absorbance was measured at 765 nm using a spectrophotometer. The phenolic content of the

sample in milligrams of gallic acid equivalent (GAE) per gram of extract was determined using the calibration curve.

2.2.4 Total Flavonoid Content Analysis

A calibration curve was obtained with a linear equation of (y = 0.0238x + 0.0064), R^2=0.9976. To determine the total flavonoid content (TFC) of each sample, 0.5 mL of extract, 2 mL of distilled water, and 0.15 mL of 50 % sodium nitrate were mixed in a test tube. The mixture was allowed to sit at room temperature for 5 minutes. Afterward, 0.15 mL of 10 % aluminum chloride was added, and the solution was incubated for 15 minutes. The absorbance of the resulting mixtures at different concentrations (20, 40, 60, and 80 ppm) was then measured at 415 nm using a spectrophotometer. The TFC of the sample in milligrams of quercetin equivalent (QE) per gram of extract was determined using the calibration curve.

2.2.5 2,2-diphenyl-1-picryhydazyl (DPPH) Free Radical Scavenging Activity

1.0 mL of the extract was combined with a DPPH solution (3.0 mL, 0.6 mM, using ethanol as the solvent). The mixture was then placed in a sealed, opaque container for 30 minutes. The absorbance was measured at a wavelength of 517 nm. The calibration standard for this measurement was an ethanol solution. To determine the radical-scavenging activity of each solution, the percentage of inhibition was substituted into Equation 2.

$$DPPH-scavenging\ activity\ (\%) = \left[\frac{A_0 - A_1}{A_0}\right] \times 100\% \quad (2)$$

2.2.6 ABTS Radical Scavenging Assay

Stock solutions were created at 7 mM for ABTS and 2.45 mM for potassium persulfate. To prepare the 7 mM ABTS radical solution, 0.096 g of ABTS powder was dissolved in 25 mL of distilled water, while for the 2.45 mM potassium persulfate stock solution, 0.016 g of potassium persulfate was dissolved in 25 mL. These stock solutions were then combined in equal amounts and allowed to react for 14 to 16 hours in darkness, resulting in a dark-colored solution. Prior to usage, this solution was diluted with methanol to achieve an absorbance of 0.706 ± 0.02 at 734 nm. A mixture containing one milliliter of ABTS solution, and one milliliter of plant extract was allowed to react for 7 minutes before measuring the absorbance at 734 nm. The ABTS radical scavenging activity was determined using Equation 3.

$$Inhibition\ (\%) = \frac{ABTS_{control} - ABTS_{sample}}{ABTS_{control}} \times 100\% \quad (3)$$

2.2.7 Statistical Analysis on MO-loaded MMT/PCL NPs Synthesis Formulation ABTS Radical Scavenging Assay

Design-Expert® Version 13 software was applied using a two-level full factorial design for designing a sequence of statistical analysis. Four (4) different input variables involving V_{aq}/V_{or} ratios (A), stirring speed (B), MMT amount (C), and the amount of MO (D). Each factor was categorized at one of two levels, with low (−1) and high (+1) levels as tabulated in Table 1. 2^4 full factorials with 16 sequences of experiments are listed in Table 2. One response was set in this study concerning encapsulation efficiency (Y). For reproducibility reasons, triple replicates were carried out on each sequence of runs. The experiment was conducted (see Figure 1) until a predetermined aqueous-to-organic phase volumetric ratio (1.5 − 10) was achieved. Upon the introduction of the organic phase to the aqueous phase, the aqueous phase quickly became cloudy and turbid. This phenomenon occurred due to the rapid exchange of two miscible solvents, i.e. Ace from the organic phase and water from the aqueous phase. Ace was then evaporated from the nanosuspension at room temperature until the smell of Ace had completely disappeared.

2.2.8 Encapsulation Efficiency Measurement

The MO-loaded MMT/PCL NPs were separated after organic solvent removal, using Beckman L-8 60M Ultracentrifuge for 1 h at 20 °C and 15 000 rpm. The supernatant containing the dissolved free drug was removed and its concentration was analyzed using a UV–visible spectrophotometer (UV-2550, Shimadzu, Japan). The sediment was then 48 h freeze-dried (Edwards Modulyo Freeze-drier) for the next physicochemical characterization. The concentration of TPC in the supernatant was then calculated using the calibration curve obtained previously. The drug encapsulation efficiency (EE) and drug loading (DL) were calculated using Equation 4.

$$EE_{TPC}\ (\%) = 1 - \frac{phenolic\ content\ on\ NPs\ surface}{phenolic\ content\ of\ NPs} \times 100\% \quad (4)$$

Table 1 Values input variables for the low (−1) and high (+1) levels of 2^4 full factorials design

Input values	Unit	Code	Low-level (–)	High-level (+)
V_{aq}/V_{or}	-	A	1.5	10
Stirring speed	rpm	B	400	1200
[a]MMT amount	wt %	C	2	5
[a]MO	wt %	D	1	5

**Note: a = Percentage values relied on the polymer amount.*

Table 2 2^4 full factorials run with the response (n = 3)

Run Order	*A*	*B*	*C*	*D*	*Y* (%)
1	1.5	400	5	1	91.60
5	1.5	1200	2	1	84.01
7	10.0	400	2	1	15.40
9	1.5	1200	5	1	28.45
10	10.0	400	5	1	52.40
13	10.0	1200	2	1	10.91
14	1.5	400	2	1	64.31
16	10.0	1200	5	1	12.34
2	10.0	400	5	5	9.12
3	1.5	400	5	5	70.51

4	10.0	400	2	5	8.63
6	10.0	1200	2	5	12.92
8	10.0	1200	5	5	10.84
11	1.5	1200	5	5	61.60
12	1.5	400	2	5	59.11

2.2.9 Physicochemical analyses of MO-loaded MMT/PCL NPs

2.2.9.1 Scanning Electron Microscopy (SEM)

3D SEM images of the fabricated NPs were acquired using an LEO model 1530 VP FEG-SEM (LEO Elektronenmikroskopie GmbH, Oberkochen, Germany). The samples were placed onto conventional aluminum sample holders with a diameter of ~1 cm. The chamber was then evacuated to ~ 0.5 Pa and the NPs images were taken using an in-lens detector operating at an accelerating voltage of 5-10 kV and a working distance of 5-10 mm.

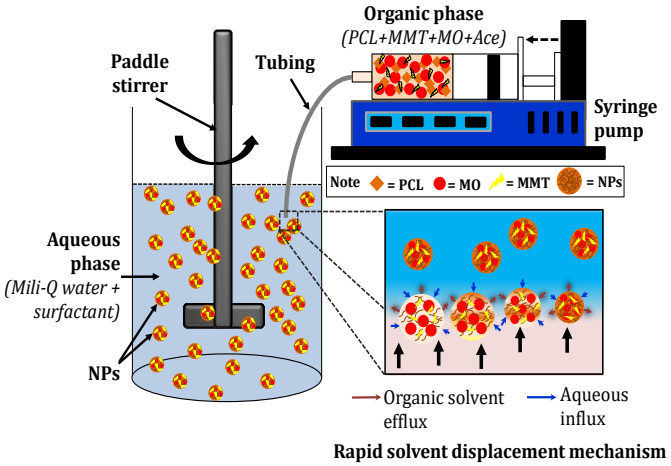

Figure 1 Experiment setup for MO-loaded MMT/PCL NPs formation

2.2.9.2 Fourier Transform Infrared Spectroscopy (FTIR)

FTIR examination was used to analyze various functional groups over the surface of blank PCL NPs, MMT/PCL NPs, MO/PCL NPs, and MO-loaded MMT/PCL NPs. Perkin Elmer FTIR Spectrum RXI Spectrometer was used to identify functional groups of prepared materials by mixing 2 mg of synthesized MO-loaded MMT/PCL NPs with 600 mg of potassium bromide (KBr). The analysis was in the spectrum absorption over the range 400-4000 cm^{-1} with a resolution of 4 cm^{-1}.

3. RESULTS AND DISCUSSION

3.1. Moisture Content of MO Leaves

MO leaves were air-dried at room temperature for 3 days and the initial moisture content was 81.96 %. After drying, the moisture content left in the leaves was 18.04 %, which was in an ideal range of 10 – 20 % to inhibit the growth of fungal and bacteria [11]. Based on Table 3, it fell in the range of studies done by Alakali et al. [13] with the same method of drying.

Table 3 Comparison of Moisture Content

Conditions	This study	Devi et al. [15]	Alqurashi & Alholaibi [13]	Alakali [14]
Drying method	Air dried	Air dried	Air dried	Under shade
Temperature	35 °C	35 °C	35 °C	35 °C
Time (days)	3	3	1	14
Moisture content (%)	81.96	-	68	84.99

3.2. TPC and TFC of MO Leaves

The extraction method of MO leaves in this study was based on the findings of Devi et al. [13] on the intensification of antioxidant-rich extract from MO leaves using different solvents. The optimized TPC and TFC values were obtained at 313.265 mg GAE/ g and 90.268 mg QE/ g respectively. However, in this current study, the TPC value was found to be higher at 386.7 mg GAE/g, indicating a higher concentration of phenolic compounds in the sample being analyzed. On the other hand, the TFC value in this study was slightly lower at 82.33 mg QE/g compared to the previous study. These results suggest that the sample in my study contains a higher amount of total phenolic compounds, while the total flavonoid content is slightly reduced compared to the optimized values reported in Devi et al. [13]. In comparison to other studies shown, which reported significantly lower values for TPC (12.47, 45.81, 127.9 mg GAE/ g) and TFC (6.71, 27.0, 73.8 mg QE/ g) than this study [14–16].

3.3. DPPH and ABTS of MO Leaves

The percentage of DPPH obtained in this study is 32.86%, which is well below the percentage obtained by Devi et al. [13] at 96.01 %. However, another study by Pakade et al. [17] shows similar results of DPPH at 40.4 %. The ABTS value obtained in this study is 49.4 %. It did not come close to the results of Devi's at 93 % or another study (70.0 – 92.48 %) [17]. Repeated experiments were conducted and yet the results remained the same and were still much lower than Devi's. The difference in the results may be due to the agroclimatic conditions [16]. The drying duration of herbs can affect the composition of the volatile component, which in turn influences their antioxidant properties. The specific constituents and their ratios, as determined by the drying duration, play a role in the observed variations in DPPH activity and ABTS [18].

3.4. Factorial Design (2^4) Analysis on MO-loaded MMT/PCL NPs

Analysis of Variance (ANOVA) was used to determine the statistical significance of the parameters such as V_{aq}/V_{org}, stirring speed, weightage of MMT, and weightage of MO. The model *F*-value of 12.02 and model *p*-value of 0.0007 imply

that there are significant differences between the parameters in the response (as summarized in Table 4). There is only a 0.07 % chance that an *F*-value this large could occur due to noise. *P*-values less than 0.0500 indicate model terms are significant. In this case, A, B, and C are significant model terms. Values greater than 0.1000 indicate the model terms are not significant such as B, C, and D. The R^2 value of 0.8890 is in reasonable agreement with the adjusted R^2 of 0.8150. The adequate precision value of 10.3599 which is greater than 4 indicates that this model has a strong signal to be used for optimization.

To determine the significance and the magnitude effects of the input variables with their significant interactions with each response were examined using analysis of variance (ANOVA). The ANOVA results are summarized in Table 5. The lack of fit of each model was believed to be statistically significant if the values of "Prob > F" were less than 0.0500. Values larger than 0.1000 imply the model terms are insignificant.

Table 4 Full factorial experimental design and response

Run Order	*A*	*B*	*C*	*D*	*Y* (%)
1	1.5	400	5	1	91.60
5	1.5	1200	2	1	84.01
7	10	400	2	1	15.40
9	1.5	1200	5	1	28.45
10	10	400	5	1	52.40
13	10	1200	2	1	10.91
14	1.5	400	2	1	64.31
16	10	1200	5	1	12.34
2	10	400	5	5	9.12
3	1.5	400	5	5	70.51
4	10	400	2	5	8.63
6	10	1200	2	5	12.92
8	10	1200	5	5	10.84
11	1.5	1200	5	5	61.60
12	1.5	400	2	5	59.11

Table 5 ANOVA test for encapsulation efficiency

Source	Sum of Squares	Mean Square	F-value	p-value	
Model	13415.53	2236	12	0.0007	significant
A	10713.29	10713	58	< 0.0001	
B	248.22	248	1.33	0.2778	
C	1.84	1.84	0.01	0.9231	
D	98.51	98.51	0.529	0.4854	
BC	1555.91	1555	8.36	0.0178	
BD	797.78	797	4.29	0.0683	
Residual	1674.72	186			
Cor Total	15090.25				

Equation 5 indicates the formula of encapsulation efficiency that can be used to make predictions for given levels of each factor.

$$EE_{TPC}\ (\%) = 65.00967 - 6.08853A + 0.021997B + 12.9225C - 8.30188D - 0.01644BC + 0.008827BD \quad (5)$$

The optimum formulations are also offered by this software as shown in Table 6. The encapsulation efficiency (% *Y*) response was set as the maximum target. This simulation strategy was applied based on the experimental results obtained by Darvishi et al. [19]. The calculated desirability factor for offered formulations was nearly 1.00 indicating the suitability of the designed factorial model. No 1 shows the selected optimum formulation for MO-loaded MMT/PCL NPs. The optimized conditions were found at a V_{aq}/V_{or} ratio of 1.5, stirring speed of 400 rpm, MMT of 5 wt%, and MO amount of 1 wt%, with an encapsulation efficiency was 91.33 % and the drug loading was 6.49 %. The accuracy of these optimized parameters was obtained at 90 % similarity by the thrice replications of actual experimental runs.

Table 6 Factorial design optimized formulations

No	A	B	C	D	Y (%)
1	**1.50**	**400**	**5.00**	**1.00**	**91.33 (selected)**
2	1.50	400	5.00	1.02	91.21
3	1.50	400	4.95	1.00	90.98
4	1.54	400	5.00	1.00	91.06
5	1.50	400	5.00	1.13	90.70
6	1.53	400	5.00	1.10	90.64
7	1.50	400	4.86	1.00	90.41
8	1.50	400	4.81	1.00	90.15
9	1.50	401	5.00	1.23	90.20
10	1.64	400	5.00	1.00	90.45
11	1.50	407	5.00	1.16	90.20
12	1.50	401	5.00	1.27	90.00
13	1.51	400	4.74	1.00	89.62
14	1.50	418	5.00	1.06	90.14
15	1.73	402	5.00	1.00	89.81

** Note: Each batch was prepared three times with No. 1 selected as the optimum formulation.*

3.5. Characterizations of MO-loaded MMT/PCL NPs

3.5.1 FTIR Spectrums

The spectrum of freeze-dried MO powder in Figure 2 depicts bands at 2921 cm^{-1} (stretching vibration of aliphatic C-H group), 2851.5 cm^{-1} (O-H stretching), 1726 cm^{-1} (C=O stretching), 1468 cm^{-1} (N=O stretching), 1238.5 cm^{-1} and 1038 cm^{-1} (C-O stretching) [20]. From the observation of Figure 2 (d), at 3625 cm^{-1}, there is an absorption band indicating the stretching vibration of the O-H bond in both the aluminum hydroxide (Al-OH) and silicon hydroxide (Si-OH) groups present in MMT. Bands at 2923 cm^{-1} and 2850 cm^{-1} can be attributed to the asymmetric and symmetric stretching of the methylene (CH_2) groups within the quaternary ammonium compound used for MMT modification. A band observed at 1467 cm^{-1} corresponds to the bending vibration of the methylene groups in the quaternary ammonium compound. Peaks around 1038 cm^{-1}, signify the stretching vibrations of the Si-O groups found in the tetrahedral sheets of MMT. Additional bands at 918.5 cm^{-1} and 886 $cm^{-1}$are associated with the bending vibrations of Al-OH, Al-Fe-OH, and Al-Mg-OH, respectively, providing further insight into the composition of MMT, as obtained by Bhagat et al. [21] and Othman et al. [10].

The IR spectrum of PCL in Figure 2 (c) shows a doublet between 2921 cm^{-1} and 2851 cm^{-1} due to the asymmetric and symmetric CH_2 stretching. Another peak shows around

1724 cm^{-1} corresponding to the carbonyl group (C=O stretching). Additional bands within the range of 700-1600 cm^{-1} are assigned to the skeletal structure of the polymer chain. These bands arise from various molecular movements, including bending, wagging, and stretching of the methylene groups. Furthermore, they indicate the presence of gauche and trans isomerization of the ester groups in the polymer. These bands provide insights into the configuration and behavior of the polymer's molecular structure, highlighting its specific characteristics and potential interactions [22].

When comparing the composite spectrum in Figure 2 (a) with the spectrum of MO powder, and pure MMT powder, there is a significant decrease in transmittance around 1000 cm^{-1} associated with the functional groups of MO and MMT [23], which suggests that the MO and MMT are encapsulated within the nanoparticles. This decrease in transmittance around was attributed to the absorption of infrared radiation by the MO and MMT particles, which are now confined within the nanoparticles. Around 1720 cm^{-1}, there is a huge increase in transmittance. This could be because the interaction between MO and PCL in the nanocomposite may result in a different molecular environment around the C=O bond compared to the individual components. The same observation has been obtained as well by Othman et al., [10], Das et al. [24], and Perumalsamy et al. [25].

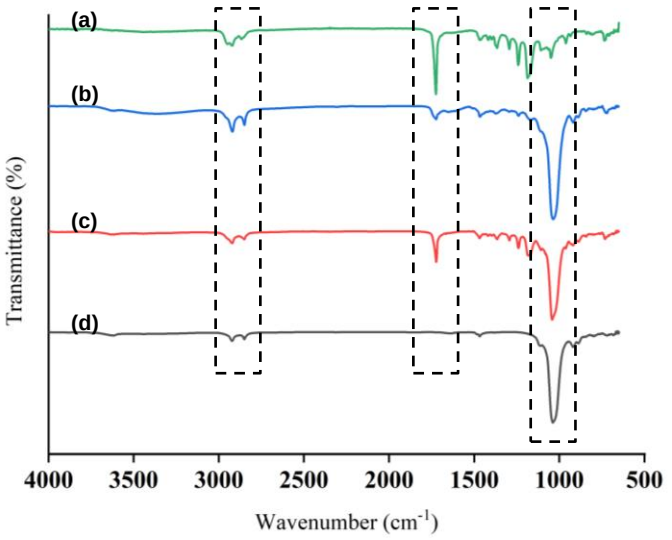

Figure 2 FTIR spectrums of (a) MO-loaded MMT/PCL NPs, (b) MO powdered extract, (c) Pure PCL, (d) Pure MMT

3.5.2 Surface Morphology of MO-loaded MMT/PCL NPs

Figure 3 (a) indicates a spherical shape of the blank PCL NPS nanoparticle at approximately 259 nm in size. Figure 3.3 (b) shows PCL nanoparticles loaded with 1 wt% MO. 1 wt% MO loaded PCL nanoparticles have an ellipse in shape and the average size is approximately 273 nm. Figure 3 (c) shows PCL nanoparticles loaded with 5 % MMT. Due to the incorporation of 5 wt% MMT in the PCL matrix, the shape of the nanoparticles is slightly distorted from the spherical shape. The average particle size of 5 wt% MMT loaded PCL is approximately 283 nm. Figure 3 (d) depicts PCL nanoparticles loaded with 5 wt% MMT and 1 wt% MO with an average particle size of 233 nm. The shape of these composite nanoparticles was a bit elongated in spherical shape due to the incorporation of MMT and MO onto the particle matrix. Similar observations have been acquired by Othman et al. [10] and Bhagat et al. [22] for the appearance of this composite particle with the inclusion of adhesive MMT and herbal MO extract.

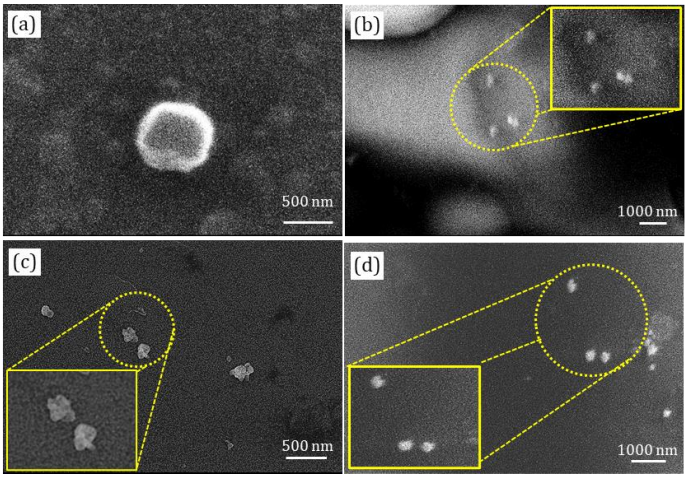

Figure 3 SEM images of; (a) Blank PCL, (b) MO-loaded PCL, (c) MMT-loaded PCL (d) MO-loaded MMT/ PCL nanoparticles.

4. CONCLUSIONS

The drying process of MO leaves achieved a moisture content range of 18.04 % left in MO leaves, falling within the desired range of 10 – 20 %. The extracted MO sample showed a higher total phenolic content (TPC) of 386.7 mg GAE/g compared to a previous study, while the total flavonoid content (TFC) was slightly lower at 82.33 mg QE/g. The antioxidant activity, measured by DPPH and ABTS assays, showed a DPPH percentage of 32.86 % and an ABTS value of 49.4 %. These results were lower than those reported in a reference study but comparable to another study. The optimized conditions for producing MO-loaded MMT/PCL nanoparticles were at a V_{aq}/V_{or} ratio of 1.5, stirring speed of 400 rpm, MMT of 5 wt%, and MO amount of 1 wt%. The expected encapsulation efficiency was 91.33 % and the drug loading was 6.49 %.

A comparison of the composite spectrum with the spectra of MO powder and pure MMT powder showed a significant decrease in transmittance around 1000 cm^{-1}, indicating encapsulation of MO and MMT within the nanoparticles. This decrease in transmittance suggested that the MO and MMT particles are confined within the nanoparticles, absorbing the infrared radiation. The blank PCL nanoparticles have a spherical shape with an average size of 259 nm. PCL nanoparticles loaded with 1 w/w % MO exhibit an elliptical shape with an average size of 273 nm. The incorporation of 5 w/w % MMT in PCL nanoparticles slightly alters the nanoparticles into a diagonal shape, and their average size increases to 283 nm. PCL nanoparticles loaded with both 5 w/w% MMT and 1 w/w% MO have an average size of 233 nm and an elliptical shape. This indicates that MMT and MO are successfully incorporated into the PCL nanoparticles matrix.

ACKNOWLEDGMENTS

The authors gratefully acknowledge the financial support given for this work through the grant FRGS/1/2021/TK0/UNIMAP/02/11.

REFERENCES

[1] A. A. Redha, S. Perna, A. Riva, G. Petrangolini, G. Peroni, M. Nichetti, G. Iannello, M. Naso, M. A. Faliva, and M. Rondanelli, "Novel insights on anti-obesity potential of the miracle tree, moringa oleifera: A systematic review," *Journal of Functional Foods*, vol. 84, p. 104600, 2021.

[2] A. S. Nugraha, R. P. Agustina, S. Mirza, D. M. Rani, N. B. Winarto, B. Triatmoko, A. N. W. Pratama, P. A. Keller, and P. Wangchuk, "Phytochemistry and Pharmacology of Medicinal Plants Used by the Tenggerese Society in Java Island of Indonesia," *Molecules*, vol. 21, pp. 1-25, 2022.

[3] D. S. Kim, M. H. Choi, and H. J. Shin, "Extracts of moringa oleifera leaves from different cultivation regions show both antioxidant and antiobesity activities," *Journal of Food Biochemistry*, vol. 44, p. e13282, 2020.

[4] B. Begines, T. Ortiz, M. Pérez-Aranda, G. Martínez, M. Merinero, F. Argüelles-Arias, and A. Alcudia, "Polymeric nanoparticles for drug delivery: recent developments and future prospects," *Nanomaterials*, vol. 10, pp. 1-41, 2020.

[5] V. Harish, D. Tewari, M. Gaur, A. B. Yadav, S. Swaroop, M. Bechelany, and A. Barhoum, "Review on Nanoparticles and Nanostructured Materials: Bioimaging, Biosensing, Drug Delivery, Tissue Engineering, Antimicrobial, and Agro-Food Applications," *Nanomaterials*, vol. 12, pp. 1-43, 2022.

[6] M. M. Ashour, M. Mabrouk, M. A. Aboelnasr, H. H. Beherei, K. M. Tohamy, and D. B. Das, "Anti-obesity drug delivery systems: recent progress and challenges," *Pharmaceutics*, vol. 15, pp. 1-42, 2023.

[7] M. N. Sardoiwala, B. Kaundal, and S. R. Choudhury, "Development of engineered nanoparticles expediting diagnostic and therapeutic applications across blood-brain barrier," in *Handbook of Nanomaterials for Industrial Applications*, pp. 696-709, 2018.

[8] R. Othman, G. T. Vladisavljević, and Z. K. Nagy, "Preparation of biodegradable polymeric nanoparticles for pharmaceutical applications using glass capillary microfluidics," *Chemical Engineering Science*, vol. 137, pp. 119-130, 2015.

[9] T. Pulingam, P. Foroozandeh, J. A. Chuah, and K. Sudesh, "Exploring various techniques for the chemical and biological synthesis of polymeric nanoparticles," *Nanomaterials*, vol. 12, pp. 1-27, 2022.

[10] R. Othman, G. T. Vladisavljević, N. L. Thomas, and Z. K. Nagy, "Fabrication of composite poly(D,L-lactide)/montmorillonite nanoparticles for controlled delivery of acetaminophen by solvent-displacement method using glass capillary microfluidics," *Colloids Surface B Biointerfaces*, vol. 141, pp. 187-195, 2016.

[11] S. J. Nikkhah and D. Thompson, "Molecular Modelling Guided Modulation of Molecular Shape and Charge for Design of Smart Self-Assembled Polymeric Drug Transporters," *Pharmaceutics*, vol. 141, pp. 1-28, 2021.

[12] R. Alqurashi and M. Alholaibi, "Polyphenols from moringa oleifera and mulberry exhibit anti-obesity and anti-hyperlipidemic effects in rats fed a high-fat diet," *Current Topics in Nutraceutical Research*, vol. 21, pp. 102-108, 2023.

[13] M. Devi, R. Othman, S. P. M. Bohari, and O. W. Jinn, "Intensification of antioxidant-rich extract from Moringa oleifera leaves using different solvents: optimization and characterization," in *Proceeding of the International Conference on Biomass Utilization and Sustainable Energy*, Springer Nature, 2022.

[14] S. H. Sathwanea, V. S. Vairagadeb, and K. S. Kenec, "Combine effect of rice husk ash and fly ash on concrete by 30% cement replacement," in *Proceeding of the International Conference on Civil Engineering*, Springer, vol. 38, no. 12, pp. 625-638, 2013.

[15] B. Vongsak, P. Sithisarn, S. Mangmool, S. Thongpraditchote, Y. Wongkrajang, and W. Gritsanapan, "Maximizing total phenolics, total flavonoids contents and antioxidant activity of Moringa oleifera leaf extract by the appropriate extraction method," *Industrial Crops and Products*, vol. 44, pp. 566-571, 2013.

[16] S. Sreelatha and P. R. Padma, "Antioxidant activity and total phenolic content of Moringa oleifera leaves in two stages of maturity," *Plant Foods for Human Nutrition*, vol. 64, pp. 303-311, 2009.

[17] V. Pakade, E. Cukrowska, and L. Chimuka, "Comparison of antioxidant activity of Moringa oleifera and selected vegetables in South Africa," *South African Journal of Science*, vol. 109, no. 3-4, 2013.

[18] M. Darvishi, S. Hasani, A. Mashreghi, M. T. Rezvan, and A. Ziarati, "Application of the full factorial design to improving the properties of CoFe2O4 nanoparticles by simultaneously adding apple cider vinegar and agarose," *Materials Science and Engineering: B*, vol. 297, pp. 1-15, 2023.

[19] M. Mostafa Ahmed, D. A. Marrez, N. M. Abdelmoeen, E. A. Mahmoud, M. A.-S. Ali, K. Decsi, and Z. Tóth, "Proximate analysis of Moringa oleifera leaves and the antimicrobial activities of successive leaf ethanolic and aqueous extracts compared with green chemically synthesized Ag-NPs and crude aqueous extract against some pathogens," *International Journal of Molecular Sciences*, vol. 24, p. 3529, 2023.

[20] S. Bhagath, A. Vivek, V. V. Krishna, S. S. Mittal, and M. Balachandran, "Synthesis and characteristics of MMT reinforced chitosan nanocomposite," *Materials Today: Proceedings*, vol. 46, pp. 4487-4492, 2021.

[21] M. E. Fortuna, E. Ungureanu, R. Rotaru, A. Bargan, O. C. Ungureanu, C. O. Brezuleanu, and V. Harabagiu, "Synthesis and Properties of Modified Biodegradable Polymers Based on Caprolactone," *Polymers*, vol. 15, pp. 1-16, 2023.

[22] S. Khalid, M. Arshad, S. Mahmood, F. Siddique, U. Roobab, M. M. A. N. Ranjha, and J. M. Lorenzo, "Extraction and quantification of Moringa oleifera leaf powder extracts by HPLC and FTIR," *Food Analytical Methods*, vol. 16, pp. 787-797, 2023.

[23] P. E. Das, I. A. Abu-Yousef, A. F. Majdalawieh, S. Narasimhan, and P. Poltronieri, "Green synthesis of encapsulated copper nanoparticles using a hydroalcoholic extract of Moringa oleifera leaves and assessment of their antioxidant and antimicrobial activities," *Molecules*, vol. 25, pp. 1-17, 2020.

[24] H. Perumalsamy, S. R. Balusamy, J. Sukweenadhi, S. Nag, D. MubarakAli, M. El-Agamy Farh, H. Vijay, and S. A. Rahimi, "Comprehensive review on Moringa oleifera nanoparticles: importance of polyphenols in nanoparticle synthesis, nanoparticle efficacy and their applications," *Journal of Nanobiotechnology*, vol. 22, pp. 1-27, 2024.